SHIMADZU
Excellence in Science

iMScope QT
Imaging Mass Microscope

Unrivaled Mass Spectrometry Imaging Platform

With unparalleled speed, sensitivity and spatial resolution, Shimadzu's **iMScope QT imaging mass microscope** clears the way to next-generation mass spectrometry imaging.

- Fast acquisition of high-mass, high-resolution images at the optical and molecular level
- Simultaneously visualize and analyze samples
- Full fusion with morphology studies
- Integration with the Q-TOF LCMS-9030 enables obtaining distribution information and quantitative data for comprehensive analysis
- Easy switching between MS imaging configuration and LCMS

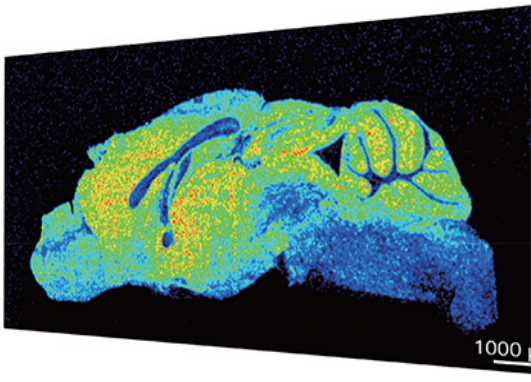

Learn more about Shimadzu's iMScope QT.

Visit us online at **www.ssi.shimadzu.com**

Shimadzu Scientific Instruments Inc., 7102 Riverwood Dr., Columbia, MD 21046, USA

McLuckey Scott (Orcid ID: 0000-0002-1648-5570)

Localization of Cyclopropyl Groups and Alkenes Within Glycerophospholipids Using Gas-Phase Ion/Ion Chemistry

De'Shovon M. Shenault, Scott A. McLuckey*, Elissia T. Franklin*

Department of Chemistry
Purdue University
560 Oval Drive
West Lafayette, IN, United States, 47907-2084

Short title: Ion/ion Rxns for Cyclopropyl Localization in GPs

*Correspondence:

Dr. Elissia T. Franklin
560 Oval Drive
Department of Chemistry
Purdue University
West Lafayette, IN 47907-2084, USA
E-mail: franklin@silentspring.org

Dr. Scott A. McLuckey
560 Oval Drive
Department of Chemistry
Purdue University
West Lafayette, IN 47907-2084, USA
E-mail: mcluckey@purdue.edu

ABSTRACT

Shotgun lipid analysis using electrospray ionization tandem mass spectrometry (ESI-MS/MS) is a common approach for the identification and characterization of glycerophohspholipids GPs. ESI-MS/MS, with the aid of collision-induced dissociation (CID),

This article has been accepted for publication and undergone full peer review but has not been through the copyediting, typesetting, pagination and proofreading process which may lead to differences between this version and the Version of Record. Please cite this article as doi: 10.1002/jms.4913

enables the characterization of GP species at the headgroup and fatty acyl sum compositional levels. However, important structural features that are often present, such as carbon-carbon double bond(s) and cyclopropane ring(s), etc., can be difficult to determine. Here, we report the use of gas-phase charge inversion reactions that, in combination with CID, allow for more detailed structural elucidation of GPs. CID of a singly deprotonated GP, $[GP - H]^-$, generates FA anions, $[FA - H]^-$. The fatty acid anions can then react with doubly-charged cationic magnesium tris-phenanthroline complex, $[Mg(Phen)_3]^{2+}$, to form charge inverted complex cations of the form $[FA - H + MgPhen_2]^+$. CID of the complex generates product ion spectral patterns that allow for the identification of carbon−carbon double bond position(s) as well as the sites of cyclopropyl position(s) in unsaturated lipids. This approach to determining both double bond and cyclopropane positions is demonstrated with GPs for the first time using standards and is applied to lipids extracted from *E. coli*.

Keywords: Glycerophospholipids; cyclopropane location; double bond location; ion/ion reactions; shotgun lipidomics

INTRODUCTION

Lipids constitute a large class of bio-molecules that play crucial roles in membrane composition, metabolism, and cellular communication.[1] Glycerophospholipids (GPs) constitute a common lipid class and are the major components of the membrane bilayer, aiding in energy storage and membrane organization.[2,3] Of the total GP content found in the *Escherichia coli* (*E. coli*) bacterial membrane, for example, 70 to 90% are composed of the GP sub-classes phosphatidylethanolamines (PEs), phosphatidylglycerols (PGs), and cardiolipins (CLs).[4] A typical GP is comprised of a glycerol backbone with two fatty acyl (FA) chains attached at the *sn*-1 and *sn*-2 positions via an ester linkage, and one of a variety of head-groups (e.g, ethanolamine, choline, serine, inositol, or glycerol) linked via an esterified phosphate to the glycerol backbone at the *sn*-3 position.[5,6] The complexity of the FA chains of GPs can vary, for example, on the basis of acyl chain length, nature of unsaturation (i.e., double bonds versus cyclopropane rings), extents of unsaturation, site(s) of unsaturation, and stereochemistry (e.g. cis- versus trans- double bonds).[7]

Electrospray ionization tandem mass spectrometry (ESI-MS/MS) has been used to address the structural complexity of GPs. Activation methods such as collision-induced dissociation (CID) or higher-energy collisional dissociation, are commonly used for the structural elucidation of GPs.[8,9] These methods applied to ions produced via ESI typically provide head-group and acyl chain composition, but are limited in localizing alterations (e.g., sites of unsaturation, cyclization, or oxidation) within the fatty acyl chain.[10] Furthermore, determining the cis/trans stereochemistry of the double bonds in lipids is problematic for widely available techniques in lipidomics,[11] although cis/trans isomers have been separated using ion mobility spectrometry and distinguished using ozone-induced dissociation (OzID) when applied to lipid standards.[11]

Although less common than double bonds, cyclopropane rings can also be present in GPs and can have significant biological relevance. Cyclopropane-containing fatty acids (CFAs), for example, are commonly found in bacteria, such as *E. coli*, *Streptococcus*, and *Salmonella*.[12] CFAs are generated by adding a methylene group, originating from S'-adenosyl-L-methionine, across the C=C bond of an unsaturated fatty acid in bacterial phospholipids.[13,14,15] The synthetic pathway of CFA has been extensively studied in *E. coli*[16] and it has been reported that CFAs increase the resistance of *E. coli* to acid stress due to their influence on membrane fluidity.[17,18] It is therefore important to be able to identify the presence

of CFAs and to localize the position(s) of the cyclopropane rings in order to understand their roles.[19]

Gas-chromatography mass spectrometry constitutes the gold standard for the elucidation of lipids containing CFAs, but can be time-consuming and is limited to volatile lipid samples.[20,21] Various approaches, such as condensed-phase derivatization with the Paternò-Büchi (PB) reaction[22] and ozone-induced dissociation (OzID),[23] have been shown to be capable of determining the site(s) of unsaturation but are not appropriate for localizing cyclopropane moieties.[22,23] Electron-based MS/MS techniques have been described for GP characterization, including double bond localization.[24,25,26,27] An ultraviolent photodissociation (UVPD) method combined with CID, recently described by Brodbelt et al., demonstrated the localization of both C=C double bonds and cyclopropane rings in GPs derived from a bacterial extract.[10,28] However, UVPD generally yields low dissociation efficiencies, which makes challenging the determination of relatively low level components in biological matrices.

In this work, we demonstrate for the first time the use of gas-phase charge inversion ion/ion reactions in conjunction with CID for the localization of cyclopropane and double bond sites in GPs. Charge inversion reactions have been demonstrated for the partial structural characterization of GPs, including the localization of double bonds, present in biological matrices.[29,30] In brief, CID of a singly deprotonated GP, $[GP\text{-}H]^-$, generates deprotonated FA anions, $[FA\text{-}H]^-$, from the fatty acyl chains. The mass of an FA anion reveals the carbon number and degree of unsaturation but CID of the anions does not reveal sites of unsaturation. The FA anions can be reacted with the doubly charged magnesium tris-phenanthroline complex, $[Mg(Phen)_3]^{2+}$, to form cations, $[FA\text{-}H+MgPhen]^+$. Subsequent CID of this ion results in charge-remote fragmentation along the aliphatic chain of the FA, which allows for the localization of double bonds and cyclopropane sites.[31] Recently, we reported the charge inversion of FA anions generated from cardiolipins to identify carbon−carbon double (C=C) bond position(s) as well as the site(s) of cyclopropyl position(s).[31,32] We demonstrate here the application of a similar strategy to localize both cyclopropane moieties and double bonds within the fatty acyl chains in a mixture comprised primarily of PE, and PG GPs. Specifically, standards of GPs with CFAs are used to demonstrate the process while GPs extracted from *E. coli* are used to demonstrate the capability of the work-flow in characterizing both double bond and cyclopropane isomers in a biological matrix.

EXPERIMENTAL SECTION

Nomenclature

The shorthand notation for lipid structures proposed by Liebisch et al. is adapted throughout this work when applicable.[33] GP classes are identified by their headgroups and abbreviated as such: e.g., phosphatidylcholine (PC), phosphatidylethanolamine (PE), and phosphatidylglycerol (PG). GP standards have identified head groups, fatty acyl carbon numbers, C=C location, degrees of unsaturation, and stereo-orientation. For example, PC 16:0/18:1(9Z) represents a GP with a PC headgroup, a FA 16:0 and FA 18:1 fatty acyl chain at the *sn*-1 and *sn*-2 positions, respectively, where the separator "/" indicating that the *sn*-positions are known. The separator "_" is used when the *sn*-positions are not known. The number before and after ":" indicate the carbon chain length and degree of unsaturation, respectively. C=C position and geometry is specified using "9Z" nomenclature meaning that the double bond is at the 9th carbon of the fatty acyl chain with cis geometry. When the C=C geometry is unknown, Δ-nomenclature followed by the carbon position number is used, i.e., PC 16:0/18:1(Δ9). C=Cs with a cyclopropane modification are described using the nomenclature proposed by Blevins et al. where "c" specifies a known cyclopropane at that position.[10] For

example, PC 16:0/18:1(c9) represents a cyclopropane motif at the 9th carbon along the fatty acyl chain of the *sn*-2 chain.

Chemicals

PE 16:1/17:1(c9) (16:0-17:0 cyclo PE (1-palmitoyl-2-cis-9,10-methylenehexadecanoyl-*sn*-glycero-3-phosphoethanolamine)), 17:1 Lyso PC (1-(10Z-heptadecenoyl)-2-hydroxy-*sn*-glycero-3-phosphocholine) standards and *E. coli* Total Lipid Extract (product #100500) were purchased from Avanti Polar Lipids (Alabaster, AL). Cis-10 nonadecanoic acid (10Z-nonadecenoic acid) (19:1(10Z)), phytomonic acid (19:1(c11)), FA 16:0, and FA 16:1(9Z) standards were purchased from Cayman Chemical Company (Ann Arbor, MI). Magnesium chloride, 1,10-phenanthroline (Phen), and HPLC Grade methanol were purchased from Thermo Fisher Scientific (Waltham, MA).

Sample Preparation

The lipid standards were dissolved in methanol and dilute to a final concentration of 10 μM. Similarly, a solution of the *E. coli* lipid extract (total) was prepared by dissolving the extract in methanol and diluted to a final concentration of 50 μM in methanol. Tris-phenanthroline magnesium complexes were prepared by mixing 1:1 (mol/mol) magnesium chloride with 1,10-phenanthroline (Phen) in 50:50 methanol:water and diluted with methanol to a final concentration of 20 μM.

Mass Spectrometry

All experiments were performed using a QTRAP 4000 hybrid triple quadrupole/linear ion-trap system (Sciex, Concord, ON, Canada). As previously reported,[34] this instrument has been modified to allow for the storage of anionic and cationic species simultaneously. Oppositely-charged ions were generated from separate nano-ESI emitters in an alternately-pulsed fashion.[35] FA standards were generated as anions using nano-ESI (-1700 V), mass selected with Q1, and transferred to the high-pressure collision cell, q2, where they were stored. Tris-phenanthroline magnesium cations, $[Mg(Phen)_3]^{2+}$, were produced by nano-ESI (+1200 V), mass isolated by Q1, and transferred to q2 to be mutually stored with the lipid fragment anions for 0.3 s.[31] The resulting cationic products, $[FA\text{-}H+Mg(Phen)_2]^+$, were transferred to Q3 where they were each mass-selected and subjected to CID. This initial CID step served to remove one of the Phen ligands to yield a $[FA\text{-}H+MgPhen]^+$ ion. Ion isolation and activation of each $[FA\text{-}H+MgPhen]^+$ ion was performed by single frequency resonance excitation at a q value of 0.383. Mass analysis was performed using mass selective axial ejection.[36] The GP anions were generated using nano-ESI (-1700 V), mass selected with Q1, and transferred to the high pressure collision cell, q2, where they were stored and subsequently collisionally activated (q=0.25) to produce fatty acyl chain fragment anions $[FA\text{-}H]^-$. The procedure described above for the anions of the FA standards to generate and characterize $[FA\text{-}H+MgPhen]^+$ ions was used for the FA anions generated from the GP anions.

RESULTS AND DISCUSSION

Distinguishing cyclopropane moieties from carbon-carbon double bonds in fatty acyl chains. Anions of model FA anions were generated by nano-ESI, converted to $[FA\text{-}H+MgPhen]^+$ ions via ion/ion reaction, and subjected to CID to illustrate the behavior of saturated, double-bond containing, and cyclopropane containing FA ions of the form $[FA\text{-}H+MgPhen]^+$. **Figure 1** highlights regions of the CID product ion spectra of (a) $[16:0\text{-}H+MgPhen]^+$, (b) $[16:1(9Z)\text{-}H+MgPhen]^+$, and (c) and $[17:1(c9)\text{-}H+MgPhen]^+$ that show the distinctive dissociation behaviors of a saturated FA, a FA with single double bond, and a FA

with a cyclopropane, respectively. With the exception of the *m/z* 262 ion, which is common to the product ion spectra of all [FA-H+MgPhen]$^+$ ions and corresponds to [•$CH_2CO_2^-$ +Mg^{2+}Phen]$^+$, all product ions containing FA fragments are even-electron. In the case of the saturated FA cations, all of the neutral losses that are complementary to the even-electron product ions are alkanes (**Figure 1(a)**). This indicates that a hydrogen transfer from the charged product to the neutral product, resulting in a double bond in the charged fragment, is the dominant process for each of the observed backbone cleavages, with the exception of the process leading to *m/z* 262. When a double bond is present, cleavages at and adjacent to the double bond are inhibited relative to cleavages one bond further away from the double bond (see **Figure 1(b)**).[37] Furthermore, spacings of 12 Da are observed between the fragments on either side of the double bond and the low-abundance fragments arising from the double bond location (compare *m/z* 359 with *m/z* 371 and *m/z* 357 with *m/z* 345) in **Figure 1(b)**).[33] The proposed products from the dissociation reactions of [16:0-H+MgPhen]$^+$ leading to these ions are provided in **Scheme 1.** Fragmentation of the CFA ion (**Figure 1(c)**) is distinct from that of the saturated FA ion (**Figure 1(a)**) and double bond-containing FA ion (**Figure 1(b)**). In this case, multiple doublets are observed (e.g., *m/z* 357/359, *m/z* 371/373, *m/z* 385/387, and *m/z* 399/401) which reflect competing cleavage mechanisms for the relevant FA bonds involving and in the vicinity of the cyclopropyl group that result in a hydrogen transfer either to or from the charged product (see **Scheme 2**). This series of doublets constitutes a signature for the presence of a cyclopropyl group.

An illustration of the process that allows for the C=C double bond and/or cyclopropane group characterization of the fatty acyl chains of GP anions is provided in **Figure 2** using PE 16:1(9Z)/17:1(c9) as a model GP. In brief, [PE 16:1(9Z)/17:1(c9)-H]$^-$ (*m/z* 728.5) was mass-selected in Q1 and transferred to q2 where it was stored and subjected to CID to form the fatty acyl chain fragment ions, [16:1(9Z)-H]$^-$ (*m/z* 457) and [17:1(c9)-H]$^-$ (*m/z* 471). Next, [$Mg(Phen)_3$]$^{2+}$ (*m/z* 282) was mass-selected in Q1 and stored with the fatty acid anions in q2 to allow for an ion/ion reaction. Attachment of [$Mg(Phen)_3$]$^{2+}$ to the fatty acyl anions resulted in the spontaneous loss of one phenanthroline, giving rise to two distinct product peaks [16:1(9Z)-H+$Mg(Phen)_2$]$^+$ (*m/z* 637) and [17:1(c9)-H+$MgPhen_2$]$^+$ (*m/z* 651). Ion-trap CID of the ions at *m/z* 637 and *m/z* 651 resulted in the loss of an additional phen, yielding ions at *m/z* 457 ([16:1(9Z)-H+MgPhen]$^+$) and *m/z* 471 ([17:1(c9)-H+MgPhen]$^+$). Consistent with previous work,[33] CID of [16:1(9Z)-H+MgPhen]$^+$ gives rise to a spectral pattern that is indictive of a double bond (12 Da spacing) in the 9th position (**Figure 2a,** highlighted in red). In contrast, CID of [17:1(c9)-H+MgPhen]$^+$ gives rise to a distinctive fragmentation pattern arising from the cyclopropyl ring in the 9th position (c9), displaying doublets between C9-C14, as highlighted in blue and shown in **Figure 2b**.

Characterization of GP species in E. coli total lipid extract

The workflow described above was applied to an *E. coli* total lipid extract for the structural elucidation of cyclopropyl and double bond-containing GPs. The vendor quoted lipid profile of 57.5% PE; 15.1% PG; 9.8% cardiolipin; 17.6% unknown provides a suitable matrix for demonstration of ion/ion reactions and MS/MS in shotgun lipid characterization. **Figure 3** shows the negative ion mass spectrum of the *E. coli* total lipid extract over the *m/z* range of 650-850, which is dominated by PE and PG anions. The most abundant PE and PG anions that were characterized in this work are indicated in red and blue, respectively.

Figure 4 illustrates the application of the ion/ion reaction approach to characterize the ion at *m/z* 733.3, tentatively identified as a PG 33:1 based on the mass.[38] **Figure 4a** shows the CID product ion spectrum of the *m/z* 733.5 anion, which shows the two most abundant fragment ions to be at *m/z* 267.2 and *m/z* 255.2. The former corresponds to the fatty acyl chain [17:1-H]$^-$ while the latter corresponds to the fatty acyl chain [16:0−H]$^-$, identifying PG 33:1 as PG 17:1_16:0. We note that there was no evidence of an isomeric species of PG 17:0_16.1 (or any other FA combination that corresponds to 33:1) due to the absence of FA signals consistent with other FA anions. The charge inversion reaction using $[Mg(Phen)_3]^{2+}$ produced two abundant product ion peaks consistent with $[16:0\text{-}H+Mg(Phen)_2]^+$ (*m/z* 638.9) and $[17:1\text{-}H+Mg(Phen)_2]^+$ (*m/z* 650.9) (**Figure 4b**.) Isolation and CID of the *m/z* 650.9 ion resulted in the additional loss of a phenanthroline (180 Da), forming the fragment ion $[17:1-H+MgPhen]^+$ (*m/z* 471.0). Isolation and activation of the $[17:1\text{-}H+MgPhen]^+$ ion resulted in a spectrum similar to that of the 17:1 standard described above in the discussion of **Figures 1** and **2**. The diagnostic product ion doublets at *m/z* 357.2/359.2, 371.2/373.2, 385.0/387.0, 399.0/401.2 and 411.2/413.0 are consistent with the FA 17:1(c9) structure characterizing the species as PG 17:1(c9)_16:0.

An example of a PE is provided by the ion at *m/z* 728.5 from **Figure 3** consistent with the presence of PE 35:2. **Figure 5a** shows the CID spectrum of the ion at *m/z* 728.5, which resulted in four product anions that correspond the complementary pairs 17:1(*m/z* 267.2)_18:1(*m/z* 281.2) and 16:1(*m/z* 253.2)_19:1(*m/z* 295.3). The CID spectrum therefore suggests the presence of a major isomer (i.e., PE 17:1_18:1) and a minor isomer (i.e., PE 16:1_19:1). After the anions of **Figure 5a** were subjected to ion/ion reactions with $[Mg(Phen)_3]^{2+}$, the fatty acyl anions were charge inverted resulting in $[16:1-H+Mg(Phen)_2]^+$ (*m/z* 637.2), $[17:1-H+Mg(Phen)_2]^+$ (*m/z* 651.2), $[18:1-H+Mg(Phen)_2]^+$ (*m/z* 665.2), $[19:1-H+Mg(Phen)_2]^+$ (*m/z* 679.1) (**Figure 5b**).

Ion-trap CID of the ions at *m/z* 637.2, 651.2, 665.2 and 679.1 resulted in an additional loss of a phenanthroline ligand resulting in the $[16:1\text{-}H+MgPhen]^+$ (*m/z* 457.2), $[17:1\text{-}H+MgPhen]^+$ (*m/z* 471.2), $[18:1\text{-}H+MgPhen]^+$ (*m/z* 485.1) and $[19:1\text{-}H+MgPhen]^+$ (*m/z* 499.0) ions. The CID product ion spectra of the four $[FA\text{-}H+MgPhen]^+$ cations listed above are provided in **Figure 6**. Consistent with **Figure 1b**, the $[16:1\text{-}H+MgPhen]^+$ precursor ion (**Figure 6a**, *m/z* 457.2) gives rise to a spectral pattern with 12 Da spacing between *m/z* 345.1 amd *m/z* 357.1 indicating a double bond at the C9 position. A similar spectral pattern was obtained from CID of the $[18:1\text{-}H+MgPhen]^+$ ion (**Figure 6c**, *m/z* 485.1), with the tell-tale 12 Da spacing between *m/z* 373.1 and *m/z* 385.1 indicating a double bond at the C11 position. Note that it is possible for there to be mixtures of ions with different positions of unsaturation but that, in these cases, a single isomer appears to be present.

The CID spectra from both $[17:1-H+MgPhen]^+$ (**Figure 6b**, *m/z* 471.2) and $[19:1\text{-}H+MgPhen]^+$ (**Figure 6d**, m/z 499.0) ions show characteristic doublet patterns, suggesting the presence of a cyclopropyl ring at the C9 and C11 positions, respectively. A deprotonated phytomonic acid standard ($[19:1(c11)\text{-}H]^-$) was charge inverted with $[Mg(Phen)_3]^{2+}$, followed by CID to produce the $[19:1(c11)\text{-}H+MgPhen]^+$ ion at *m/z* 499.0. Another round of CID was then employed resulting in similar doublet patterns at 385.0/387.0, 399.0/401.1, 413.0/415.0, 426.9/429.1 and 441.0/443.0 to the profiled 19:1 fatty acyl chain (compare **Figure S-1** and **Figure 6d**). In contrast, cis-10-nonadecanoic acid (FA 19:1 (10Z)) was subjected to the same

process and the resulting product ion spectrum of $[19:1(10Z)\text{-}H+MgPhen]^+$ (*m/z* 499.0) shows the expected fragmentation pattern for an FA with a double bond at C10 and distinct from that of the profiled 19:1(c9) fatty acyl chain (compare **Figure S-2** with **Figure 6d**). A $[17:1(9Z)\text{-}H]^-$ anion could be generated from a lyso-PC 17:1(9Z) standard (see **Figure S-3**) to compare with the data for the profiled *m/z* 471.2 ion (compare **Figure S-3** with **Figure 6b**). The CID product ion spectrum of the *m/z* 471.2 generated from the lyso-PC 17:1(9Z) standard shows the expected pattern and 12 Da spacing for a double bond at the C9 position, in contrast with the behavior noted for the profiled *m/z* 471 ion.

Table 1 summarizes unsaturated GPs represented in the negative ion ESI mass spectrum of the *E. coli* total lipid extract (**Figure 3**) that were subjected characterization using the MS^n workflow outlined in **Figure 2**. Many of the GP anions derived from the *E. coli* extract were found to be comprised of mixtures of FA compositions, as illustrated above for the PE 35:2 ions. In a few cases, FA anions from minor components were apparent upon CID of the GP precursor anions but were too low in abundance (<2% of the most abundant FA anion generated by CID of the GP anion) to allow for subsequent isolation and CID to localize the unsaturation. These cases are indicated with an asterisk in **Table 1**.

CONCLUSION

In this work, we demonstrate for the first time the localization of both double bonds and cyclopropane sites in GPs using ion/ion charge inversion reactions. GP anions were fragmented generating FA anions in high relative abundance, which enables the identification of carbon number and the number of alkene/cyclopropyl groups. CID of deprotonated FAs, however, neither distinguishes cyclopropyl groups from double bonds nor allows for the localization of the sites of such groups. We therefore charge invert the FA anions via reaction with $[MgPhen_3]^{2+}$ initially to produce $[FA - H + Mg(Phen)_2]^+$ cations. CID of $[FA - H + Mg(Phen)_2]^+$ leads to loss of one Phen ligand, generating a $[FA - H + MgPhen]^+$ cation. CID of the $[FA - H + MgPhen]^+$ cation yields distinct fragmentation patterns for FA anions with double bonds and cyclopropyl groups. In each case, it is possible to identify whether the FA modification is a double bond or cyclopropane group as well as to localize the modification site. The phenomenology is demonstrated here with standards and is extended to GP anions generated from a *E. coli* total extract. The 16:1 and 18:1 fatty acyl chains in the *E. coli* total extract were found to be 16:1 (Δ9) and 18:1 (Δ11), respectively, while 17:1 and 19:1 fatty acyl chains were found to be 17:1 (c9) and 19 (c11), respectively. The demonstrated work-flow offers extensive GP structural characterization using gas-phase ion/ion reactions and tandem mass spectrometry.

ACKNOWLEDGEMENTS

This work was supported by the National Institute of Health (NIH) under Grants GM R37-45372 and GM R01-118484.

DATA AVAILABILITY STATEMENT

The data that support the findings of this study are available from the corresponding author upon reasonable request.

ORCID

De'Shovon M. Shenault - orcid.org/0000-0002-9208-0655; Email: dshenaul@purdue.edu
Scott A. McLuckey - orcid.org/0000-0002-1648-5570; Email: mcluckey@purdue.edu
Elissia T. Franklin - orcid.org/0000-0002-1017-9927; Email: franklin@silentspring.org

Supporting Information
Additional supporting information can be found online in the Supporting Information section at the end of this article.

Credit Author Statement
De'Shovon Shenault: Investigation, data curation, methodology, visualization, writing - original draft preparation. **Scott A. McLuckey:** Methodology, resources, supervision, visualization, writing – review and editing. **Elissia Franklin:** Conceptualization, methodology, project administration, visualization, writing – review and editing.

Notes
The authors declare no competing financial interests.

References

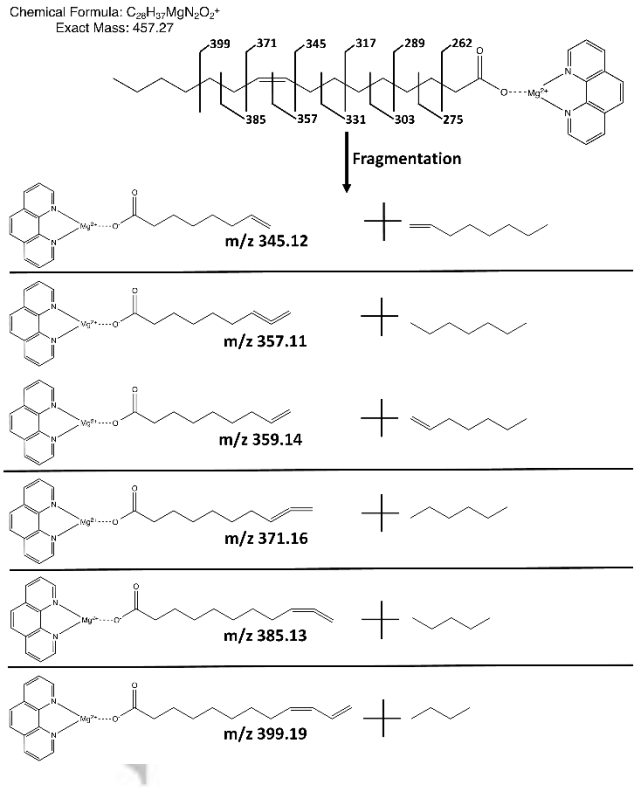

Scheme 1 – Proposed products from cleavages in the double bond region of [16:1(9Z)-H+MgPhen]$^+$

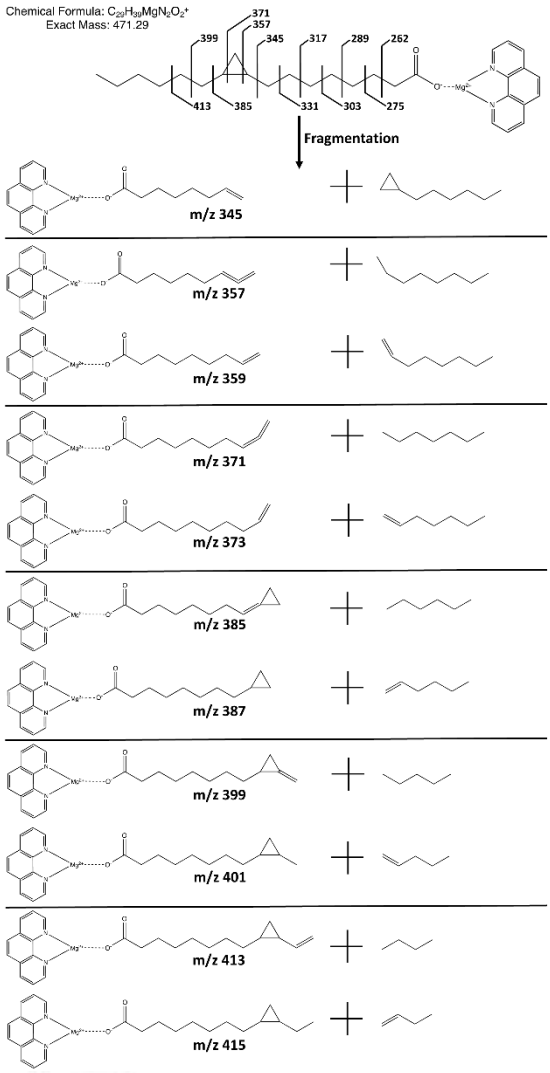

Scheme 2 – Proposed products from cleavages in the cyclopropyl region of [17:1(c9)-H+MgPhen]$^+$.

and (c) [17:1(c9)-H+MgPhen]$^+$. Filled and open circles (●/○) represent selected/unselected anions, respectively, and filled and open squares (■/□) represent selected and unselected cations. Lightning bolts (↯) indicate the precursor ion subjected to collisional activation.

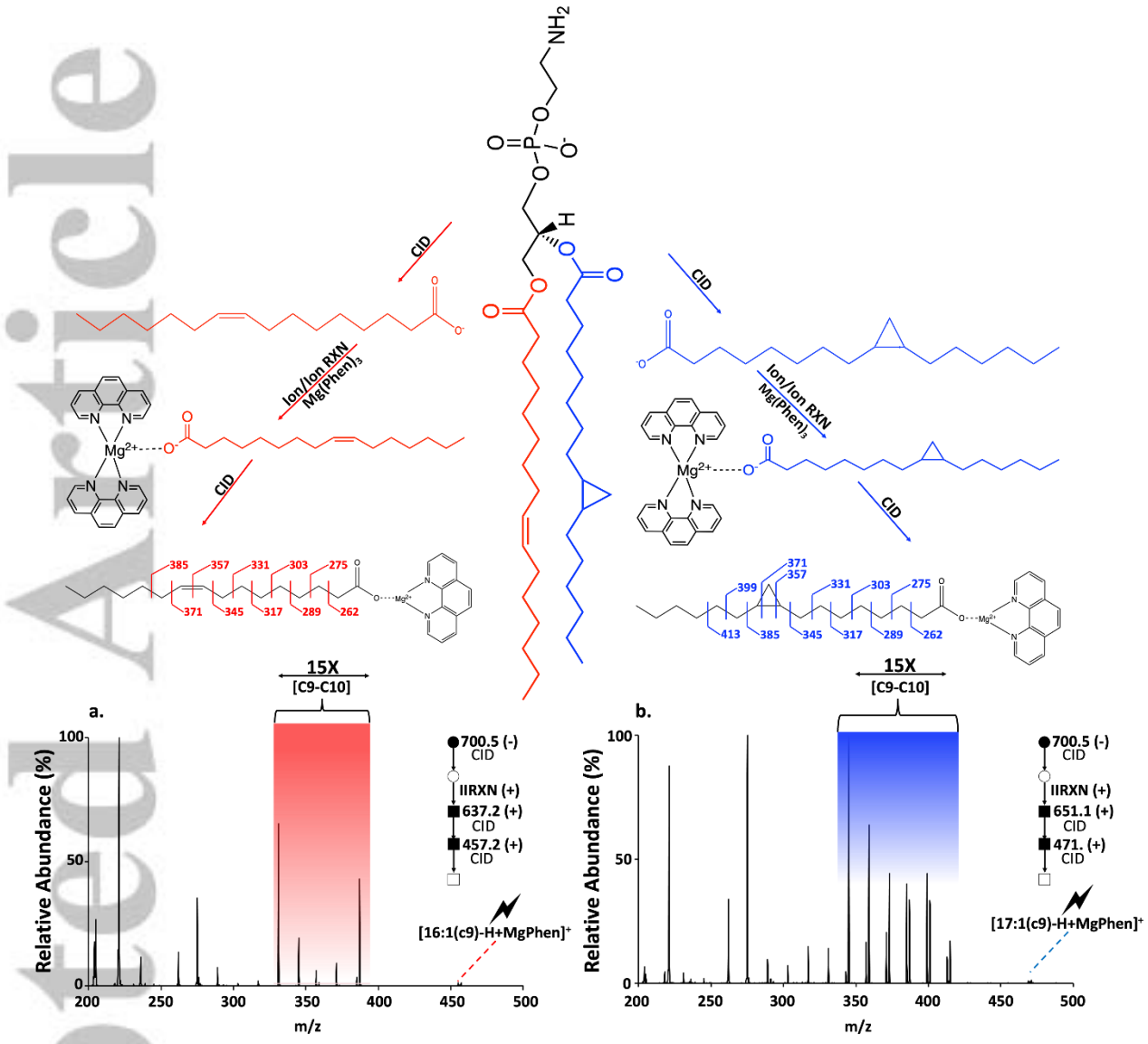

Figure 2. Graphic representation of the approach to characterize fatty acyl chains in GPs. Anionic glycerophospholipids, $[GP-H]^-$ subjected to CID generate fatty acyl anions, $[FA-H]^-$. The fatty acid anions undergo ion/ion reactions with tris-phenanthroline magnesium dictations, $[MgPhen_3]^{2+}$, resulting in a complex that spontaneously loses one of the phenanthroline ligands to yield $[FA-H+MgPhen_2]^+$ cations. Following an additional CID step to drive off a second phenanthroline ligand, CID of the resulting $[FA-H+MgPhen]^+$ cations generate product ion spectra that allow for the localization of a double bond or cyclopropyl group. Filled and open circles (●/○) represent selected/unselected anions, respectively, and filled and open squares (■/□) represent selected and unselected cations. Lightning bolts (↯) indicate the precursor ion subjected to collisional activation.

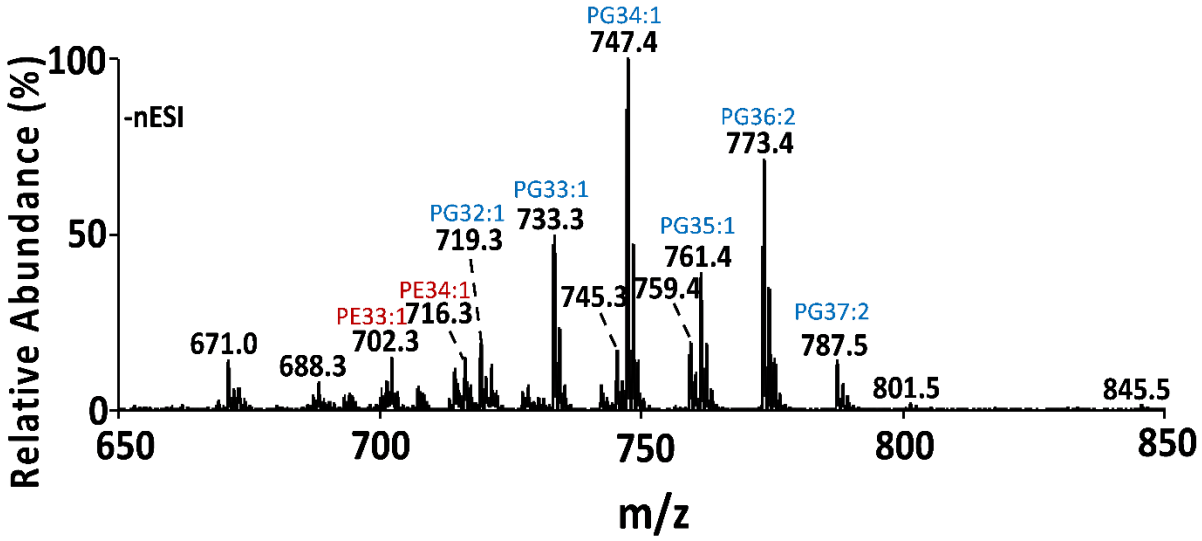

Figure 3. Negative ion mode nanoESI MS spectrum of lipid total extract from *E. coli*. Some of the mixture components that were subjected to characterization (see Table 1) are also indicated by head group, total FA carbon number and degree of unsaturation.

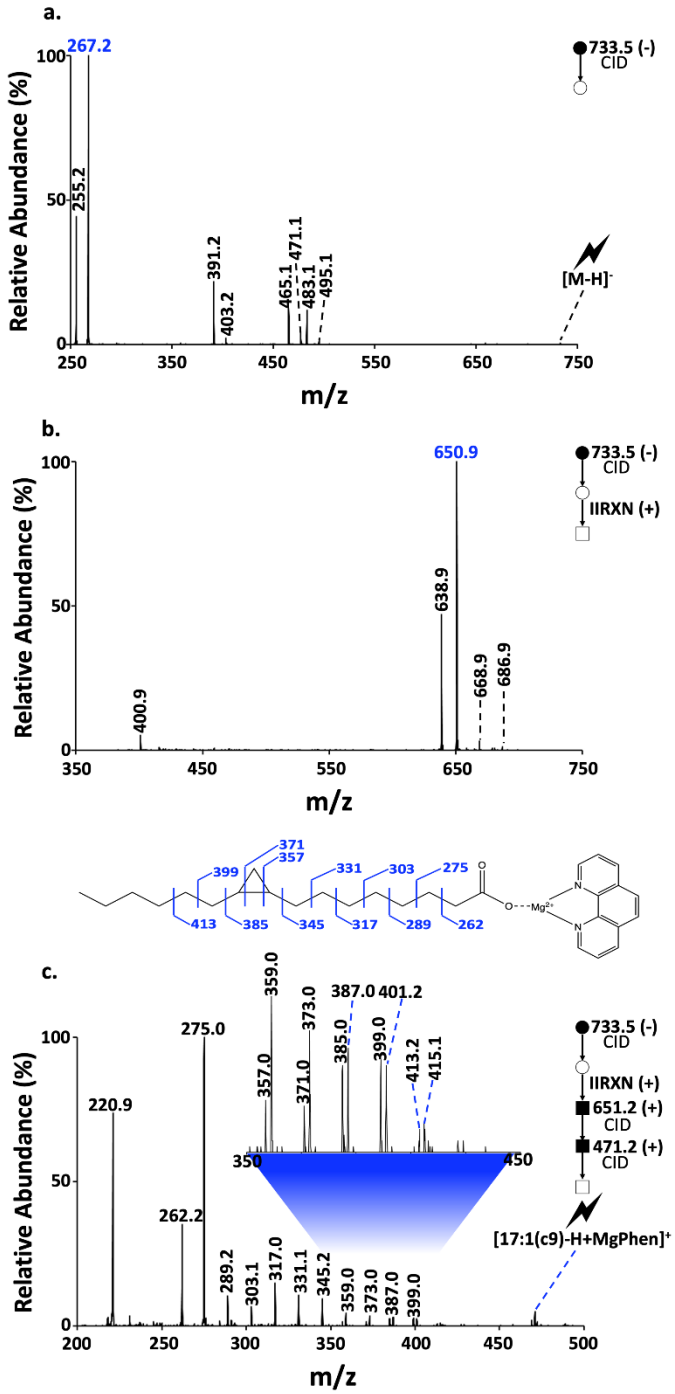

Figure 4. a) CID product ion spectrum of the PG 33:1 anion at *m/z* 733.3 (from **Figure 3**). b) Ion/ion reaction of the ions in panel a). CID of the ion at *m/z* 650.9 generates an abundant ion at m/z 471.2 (phenanthroline loss), the CID product ion spectrum of which is given in c). Filled and open circles (●/○) represent selected/unselected anions, respectively, and filled and open squares (■/□) represent selected and unselected cations. Lightning bolts (↯) indicate the precursor ion subjected to collisional activation.

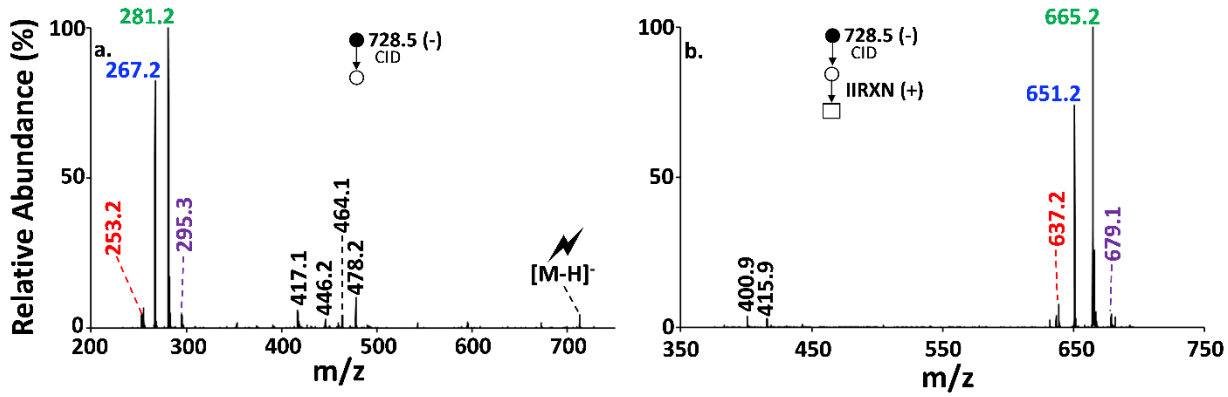

Figure 5 – (a) CID product ion spectrum of the PE 35:2 ions at m/z 728.5. (b) Product ion spectrum after reaction of the anions in (a) with $[Mg(Phen)_3]^{2+}$. Filled and open circles (●/○) represent selected/unselected anions, respectively, and filled and open squares (■/□) represent selected and unselected cations. Lightning bolts (↯) indicate the precursor ion subjected to collisional activation.

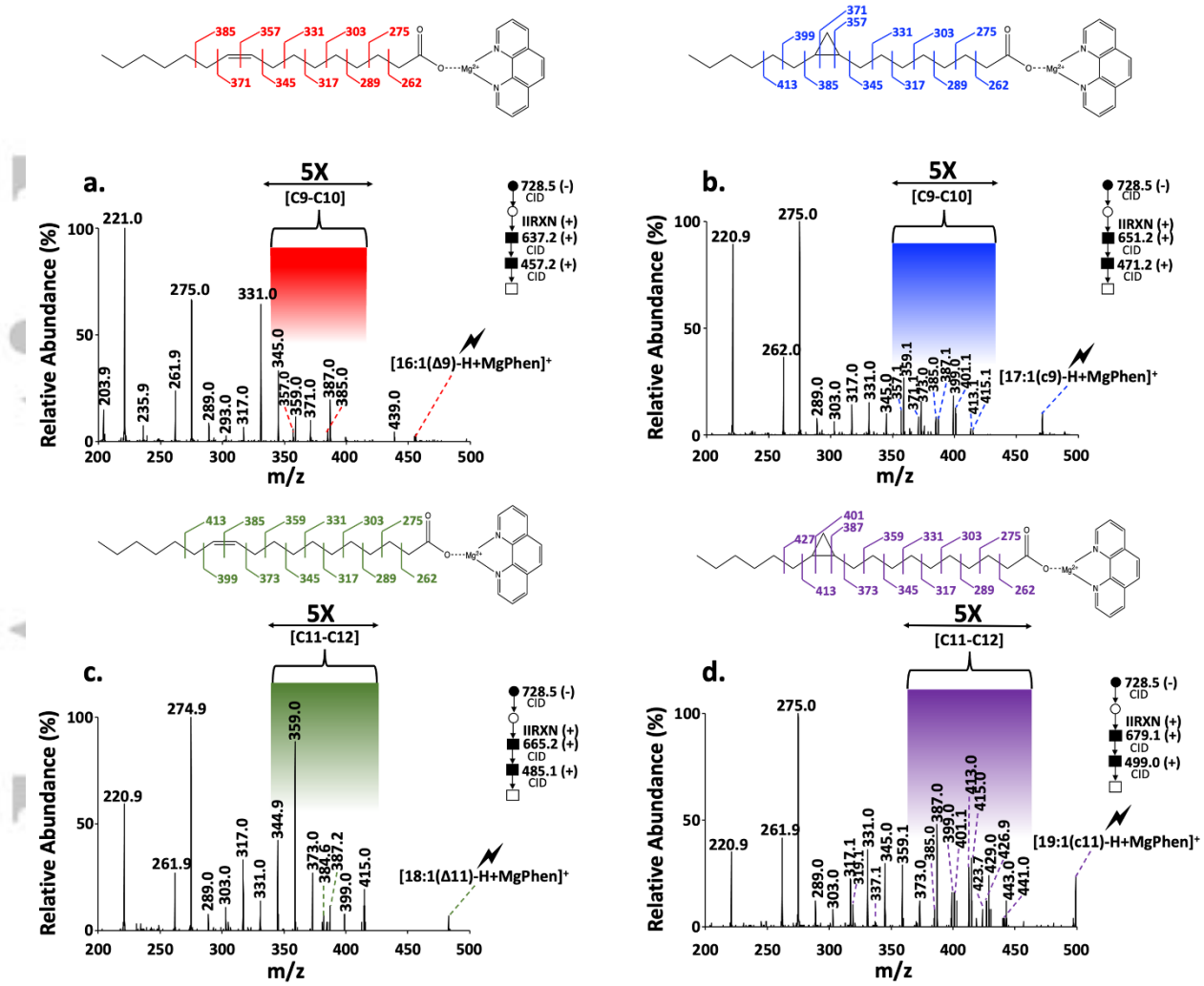

Figure 6. a) CID of the ion population at *m/z* 637.2 followed by activation of the ions at *m/z* 457.2. b) CID of the ion population at *m/z* 637.2 followed activation of the ions at *m/z* 471.2. c) CID of the ion population at *m/z* 637.2 followed by activation of the ions at *m/z* 485.1. d) CID of the ion population at *m/z* 637.2 followed by activation of the ions at *m/z* 499.0. Filled and open circles (●/○) represent selected/unselected anions, respectively, and filled and open squares (■/□) represent selected and unselected cations. Lightning bolts (↯) indicate the precursor ion subjected to collisional activation.

Headgroup	Sum Composition	Combination	m/z [M – H]$^-$	Ring Position	Double Bond Position
Standards					
PE	33:1	16:0/17:1	702.9	[17:1(c9)-H]$^-$	
PC	17:1	17:1 Lyso	542.0		[17:1(Δ10)-H]$^-$
Fatty Acid	19:1	19:1	295.6		[19:1(Δ10)-H]$^-$
Fatty Acid	19:1	19:1	295.6	[19:1(c11)-H]$^-$	
E. coli					
PE	33:2	16:1_17:1	700.5	[17:1(c9)-H]$^-$	[16:1(Δ9)-H]$^-$
"	33:2	15:1_18:1	700.5	*	[18:1(Δ11)-H]$^-$
"	33:1	16:0_17:1	702.5	[17:1(c9)-H]$^-$	
"	33:1	17:0_16:1	702.5		[16:1(Δ9)-H]$^-$
"	34:2	17:1_17:1	714.5	[17:1(c9)-H]$^-$	
"	34:2	16:1_18:1	714.5		[18:1(Δ11)-H]$^-$ [16:1(Δ9)-H]$^-$
"	34:2	15:1_19:1	714.5	[19:1(c11)-H]$^-$	*
"	34:1	16:0_18:1	716.4		[18:1(Δ11)-H]$^-$
"	34:1	16:1_18:0	716.4		[16:1(Δ9)-H]$^-$
"	34:1	17:0_17:1	716.4	[17:1(c9)-H]$^-$	
"	35.2	18:1_17:1	728.5	[17:1(c9)-H]$^-$	[18:1(Δ11)-H]$^-$
"	35.2	16:1_19:1	728.5	[19:1(c11)-H]$^-$	[16:1(Δ9)-H]$^-$
"	35:1	16:0_19:1	730.5	[19:1(c11)-H]$^-$	
"	35:1	18:0_17:1	730.5	[17:1(c9)-H]$^-$	
"	36:2	19:1_17:1	742.5	[19:1(c11)-H]$^-$ [17:1(c9)-H]$^-$	
"	36:2	18:1_18:1	742.5		[18:1(Δ11)-H]$^-$
"	37:2	17:1_20:1	756.5	[17:1(c9)-H]$^-$	
"	37:2	18:1_19:1	756.5	[19:1(c11)-H]$^-$	[18:1(Δ11)-H]$^-$
"	37:2	19:0_18:2	756.5	*	*
PG	32:1	16:0_16:1	719.4		[16:1(Δ9)-H]$^-$
"	32:1	14:0_18:1	719.4		[18:1(Δ11)-H]$^-$
"	33:1	16:0_17:1	733.4	[17:1(c9)-H]$^-$	
"	33:2	16:1_17:1	731.4	[17:1(c9)-H]$^-$	[16:1(Δ9)-H]$^-$
"	33:2	14:1_19:1	731.4	[19:1(c11)-H]$^-$	*
"	34:2	16:1_18:1	745.4		[16:1(Δ9)-H]$^-$ [18:1(Δ11)-H]$^-$
"	34:2	17:1_17:1	745.4	[17:1(c9)-H]$^-$	
"	34:1	16:0_18:1	747.5		[18:1(Δ11)-H]$^-$
"	35.2	18:1_17:1	759.5	[17:1(c9)-H]$^-$	[18:1(Δ11)-H]$^-$
"	35.2	16:1_19:1	759.5	[19:1(c11)-H]$^-$	[16:1(Δ9)-H]$^-$
"	35:1	18:0_17:1	761.5	[17:1(c9)-H]$^-$	
"	35:1	17:0_18:1	761.5		[18:1(Δ11)-H]$^-$

Table 1. The PGs and PEs in an *E. coli* total lipid extract characterized via MS^n involving CID of the deprotonated GP, ion/ion charge inversion of the FA product anions using tris-phenanthroline magnesium dictations, and CID of the $[FA-H+MgPhen]^+$ ions. Asterisks

indicate cases in which the FA anions could be observed from minor GP components but were too low in abundance for further characterization via MS/MS.

[1] A. Naudí, R. Cabré, M. Jové, V. Ayala, H. Gonzalo, M. Portero-Otín, I. Ferrer, R. Pamplona. Chapter Five - Lipidomics of Human Brain Aging and Alzheimer's Disease Pathology. In *International Review of Neurobiology*; Hurley, M. J., Ed.; Omic Studies of Neurodegenerative Disease: Part B; Academic Press, 2015; Vol. 122, pp 133–189. https://doi.org/10.1016/bs.irn.2015.05.008.

[2] M.C.F. Messias, G.C. Mecatti, D.G. Priolli, P. de Oliveira Carvalho. Plasmalogen Lipids: Functional Mechanism and Their Involvement in Gastrointestinal Cancer. *Lipids in Health and Disease* **2018**, *17* (1), 41. https://doi.org/10.1186/s12944-018-0685-9.

[3] J.M. Dean, I.J. Lodhi. Structural and Functional Roles of Ether Lipids. *Protein Cell* **2018**, *9* (2), 196–206. https://doi.org/10.1007/s13238-017-0423-5.

[4] A.J. De Siervo. Alterations in the Phospholipid Composition of *Escherichia coli* B During Growth at Different Temperatures. *J. Bacteriol.* **1969**, *100* (3), 1342–1349. https://doi.org/10.1128/jb.100.3.1342-1349.1969.

[5] B.Y. Tao. Chapter 24 - Industrial Applications for Plant Oils and Lipids. In *Bioprocessing for Value-Added Products from Renewable Resources*; Yang, S.-T., Ed.; Elsevier: Amsterdam, 2007; pp 611–627. https://doi.org/10.1016/B978-044452114-9/50025-6.

[6] A. Blanco, G. Blanco. Chapter 5 - Lipids. In *Medical Biochemistry*; Blanco, A., Blanco, G., Eds.; Academic Press, 2017; pp 99–119. https://doi.org/10.1016/B978-0-12-803550-4.00005-7.

[7] T.A. Garrett, C.R.H. Raetz, T. Richardson, R. Kordestani, J.D. Son, R.L. Rose. Identification of Phosphatidylserylglutamate: A Novel Minor Lipid in Escherichia coli. *Journal of Lipid Research* **2009**, *50* (8), 1589–1599. https://doi.org/10.1194/jlr.M800549-JLR200.

[8] F.-F. Hsu, J. Turk. Electrospray Ionization with Low-Energy Collisionally Activated Dissociation Tandem Mass Spectrometry of Glycerophospholipids: Mechanisms of Fragmentation and Structural Characterization. *J. Chromatogr. B* **2009**, *877* (26), 2673–2695. https://doi.org/10.1016/j.jchromb.2009.02.033.

[9] F.-F. Hsu, J. Turk. Electrospray Ionization/Tandem Quadrupole Mass Spectrometric Studies on Phosphatidylcholines: The Fragmentation Processes. *J. Am. Soc. Mass Spectrom.* **2003**, *14* (4), 352–363. https://doi.org/10.1016/S1044-0305(03)00064-3.

[10] M.S. Blevins, D.R. Klein, J.S. Brodbelt. Localization of Cyclopropane Modifications in Bacterial Lipids via 213 Nm Ultraviolet Photodissociation Mass Spectrometry. *Anal. Chem.* **2019**, *91* (10), 6820–6828. https://doi.org/10.1021/acs.analchem.9b01038.

[11] S.E. Hancock, B.L.J. Poad, A. Batarseh, S.K. Abbott, T.W. Mitchell. Advances and Unresolved Challenges in the Structural Characterization of Isomeric Lipids. *Anal. Biochem.* **2017**, *524*, 45–55. https://doi.org/10.1016/j.ab.2016.09.014.

[12] D.W. Grogan, J.E. Cronan. Cyclopropane Ring Formation in Membrane Lipids of Bacteria. *Microbiol. Mol. Biol. Rev.* **1997**, *61* (4), 429–441.

[13] D. Poger, A.E. Mark. A Ring to Rule Them All: The Effect of Cyclopropane Fatty Acids on the Fluidity of Lipid Bilayers. *J. Phys. Chem. B* **2015**, *119* (17), 5487–5495. https://doi.org/10.1021/acs.jpcb.5b00958.

[14] A.Y. Wang, D.W. Grogan, J.E. Cronan. Cyclopropane Fatty Acid Synthase of Escherichia coli: Deduced Amino Acid Sequence, Purification, and Studies of the Enzyme Active Site. *Biochemistry* **1992**, *31* (45), 11020–11028. https://doi.org/10.1021/bi00160a011.

[15] Y.-M. Zhang, C.O. Rock. Membrane lipid homeostasis in bacteria. *Nat. Rev. Microbiol.* **2008**, *6*, 222–233. https://www.nature.com/articles/nrmicro1839

[16] M.S. Glickman, S.M. Cahill, W.R. Jacobs. The Mycobacterium Tuberculosis CmaA2 Gene Encodes a Mycolic Acid Trans-Cyclopropane Synthetase. *J. Biol. Chem.* **2001**, *276* (3), 2228–2233. https://doi.org/10.1074/jbc.C000652200.

[17] Y.Y. Chang, J.E. Cronan. Membrane Cyclopropane Fatty Acid Content Is a Major Factor in Acid Resistance of Escherichia coli. *Mol. Microbiol.* **1999**, *33* (2), 249–259. https://doi.org/10.1046/j.1365-2958.1999.01456.x.

[18] C. Xu, S. Wang, H. Ren, X. Lin, L. Wu, X. Peng. Proteomic Analysis on the Expression of Outer Membrane Proteins of Vibrio Alginolyticus at Different Sodium Concentrations. *PROTEOMICS* **2005**, *5* (12), 3142–3152. https://doi.org/10.1002/pmic.200401128.

[19] P.M. Wehrli, T.B. Angerer, A. Farewell, J.S. Fletcher, J. Gottfries. Investigating the Role of the Stringent Response in Lipid Modifications during the Stationary Phase in *E. coli* by Direct Analysis with Time-of-Flight-Secondary Ion Mass Spectrometry. *Anal. Chem.* **2016**, *88* (17), 8680–8688. https://doi.org/10.1021/acs.analchem.6b01981.

[20] D.J. Harvey. Picolinyl Derivatives for the Characterization of Cyclopropane Fatty Acids by Mass Spectrometry. *Biomed. Mass Spectrom.* **1984**, *11* (4), 187–192. https://doi.org/10.1002/bms.1200110410.

[21] D. Oursel, C. Loutelier-Bourhis, N. Orange, S. Chevalier, V. Norris, C.M. Lange. Identification and relative quantification of fatty acids in Escherichia coli membranes by gas chromatography/mass spectrometry. *Rapid Commun. Mass Spectrom.* **2007**, *21(20)*, 3229-3233. https://doi: 10.1002/rcm.3177.

[22] X. Ma, Y. Xia. Pinpointing Double Bonds in Lipids by Paternò-Büchi Reactions and Mass Spectrometry. *Angew. Chem. Int. Ed.* **2014**, *53* (10), 2592–2596. https://doi.org/10.1002/anie.201310699.

[23] H.T. Pham, A.T. Maccarone, M.C. Thomas, J.L. Campbell, T.W. Mitchell, S.J. Blanksby. Structural Characterization of Glycerophospholipids by Combinations of

Ozone- and Collision-Induced Dissociation Mass Spectrometry: The next Step towards "Top-down" Lipidomics. *Analyst* **2013**, *139* (1), 204–214. https://doi.org/10.1039/C3AN01712E.

[24] J.L. Campbell, T. Baba. Near-complete structural characterization of phosphatidylcholines using electron impact excitation of ions from organics. *Anal. Chem.* **2015**, *87* (11), 5837–5845.

[25] J.W. Jones, C.J. Thompson, C.L. Carter, M.A. Kane. Electron-induced dissociation (EID) for structure characterization of glycerophosphatidylcholine: determination of double bond positions and localization of acyl chains. *J. Mass Spectrom*. **2015**, *50* (12), 1327-1339.

[26] T. Baba, J.L. Campbell, J.C.Y. Le Blanc, P.R.S. Baker, Distinguishing cis and trans isomers in intact complex lipids using electron impact excitation of ions from organics mass spectrometry. *Anal. Chem.* **2017**, *89* (14), 7307–7315.

[27] M.E.N. Born, B.M. Prentice. Structural elucidation of phosphatidylcholines from tissue using electron induced dissociation. *Int. J. Mass Spectrom.* **2020**, *452*, 11638.

[28] L.A. Macias, C.L. Feider, L.S. Eberlin, J.S. Brodbelt. Hybrid 193 nm Ultraviolet Photodissociation Mass Spectrometry Localizes Cardiolipin Unsaturations. *Anal. Chem.* **2019**, 91(19), 12509-12516. https://pubs.acs.org/doi/10.1021/acs.analchem.9b03278

[29] C.E. Randolph, S.J. Blanksby, S.A. McLuckey. Toward Complete Structure Elucidation of Glycerophospholipids in the Gas Phase through Charge Inversion Ion/Ion Chemistry. *Anal. Chem.* **2020**, *92* (1), 1219–1227. https://doi.org/10.1021/acs.analchem.9b04376.

[30] C.E. Randolph, D.M. Shenault, S.J. Blanksby, S.A. McLuckey. Structural Elucidation of Ether Glycerophospholipids Using Gas-Phase Ion/Ion Charge Inversion Chemistry. *J. Am. Soc. Mass Spectrom.* **2020**, *31* (5), 1093–1103. https://doi.org/10.1021/jasms.0c00025.

[31] C.E. Randolph, D.M. Shenault, S.J. Blanksby, S.A. McLuckey. Localization of Carbon–Carbon Double Bond and Cyclopropane Sites in Cardiolipins via Gas-Phase Charge Inversion Reactions. *J. Am. Soc. Mass Spectrom.* **2021**, *32* (2), 455–464. https://doi.org/10.1021/jasms.0c00348.

[32] C.E. Randolph, D.J. Foreman, S.J. Blanksby, S.A. McLuckey. Generating Fatty Acid Profiles in the Gas Phase: Fatty Acid Identification and Relative Quantitation Using Ion/Ion Charge Inversion Chemistry. *Anal Chem* **2019**, *91* (14), 9032–9040. https://doi.org/10.1021/acs.analchem.9b01333.

[33] G. Liebisch, E. Fahy, J. Aoki, E.A. Dennis, T. Durand, C.S. Ejsing, M. Fedorova, I. Feussner, W.J. Griffiths, H. Köfeler, A.H. Merrill, Jr., R.C. Murphy, V.B. O'Donnell, O. Oskolkova, S. Subramaniam, M.J.O. Wakelam, F. Spener. Update on LIPID MAPS classification, nomenclature, and shorthand notation for MS-derived lipid structures. *J. Lipid Res.* **2020**, *61*, 1539-1555

[34] Y. Xia, J. Wu, S.A. McLuckey, F.A. Londry, J.W. Hager. Mutual Storage Mode Ion/Ion Reactions in a Hybrid Linear Ion Trap. *J. Am. Soc. Mass Spectrom.* **2005**, *16* (1), 71–81. https://doi.org/10.1016/j.jasms.2004.09.017.

[35] Y. Xia, X. Liang, S.A. McLuckey. Pulsed Dual Electrospray Ionization for Ion/Ion Reactions. *J Am Soc Mass Spectrom* **2005**, *16* (11), 1750–1756. https://doi.org/10.1016/j.jasms.2005.07.013.

[36] F.A. Londry, J.W. Hager. Mass Selective Axial Ion Ejection from a Linear Quadrupole Ion Trap. *J. Am. Soc. Mass Spectrom.* **2003**, *14* (10), 1130–1147. https://doi.org/10.1016/S1044-0305(03)00446-X.

[37] C.E. Randolph, D.J. Foreman, S.K. Betancourt, S.J. Blanksby, S.A. McLuckey. Gas-phase Ion/ion Reactions involving tris-Phenanthroline Alkaline Earth Metal Complexes as Charge Inversion Reagents for the Identification of Fatty Acids. *Anal. Chem.* **2018**, *90*, 12861-12869. 10.1021/acs.analchem.8b03441

[38] https://www.lipidmaps.org/databases/lmsd/browse